7-13-2017

Antimicrobial Hydroxyapatite-Gelatin-Silica Composite Pastes with Tunable Setting Properties

Vuk Uskoković
Chapman University, uskokovi@chapman.edu

Shreya Ghosh
University of Illinois at Chicago

Victoria M. Wu
Chapman University

Follow this and additional works at: https://digitalcommons.chapman.edu/pharmacy_articles

Part of the Bacteriology Commons, Biomedical and Dental Materials Commons, Chemical Actions and Uses Commons, Musculoskeletal System Commons, Other Chemicals and Drugs Commons, Pharmaceutical Preparations Commons, and the Surgical Procedures, Operative Commons

Recommended Citation

Antimicrobial Hydroxyapatite-Gelatin-Silica Composite Pastes with Tunable Setting Properties

Comments

This is a pre-copy-editing, author-produced PDF of an article accepted for publication in *Journal of Materials Chemistry B*, volume 30, in 2017following peer review. The definitive publisher-authenticated version is available online at DOI: 10.1039/C7TB01794D.

Copyright

Royal Society of Chemistry

Antimicrobial Hydroxyapatite-Gelatin-Silica Composite Pastes with Tunable Setting Properties

Vuk Uskoković[1], Shreya Ghosh[2], Victoria M. Wu[1]

[1] Advanced Materials and Nanobiotechnology Laboratory, Department of Biomedical and Pharmaceutical Sciences, Center for Targeted Drug Delivery, Chapman University School of Pharmacy, 9401 Jeronimo Road, Irvine, CA 92618-1908, USA

[2] Advanced Materials and Nanobiotechnology Laboratory, Department of Bioengineering, University of Illinois, Chicago, IL 60607-7052, USA

Abstract Bone grafting is one of the commonest surgical procedures, yet all bone substitutes developed so far suffer from specific weaknesses and the search for a bone graft material with ideal physical and biological properties is still ongoing. Calcium phosphate pastes are the most frequently used synthetic bone grafts, yet they (a) often take an impractically long time to set, (b) release the drug content too fast, and (c) do not form pores large enough to accommodate host cells and foster osseointegration. To make up for these deficiencies, we introduced gelatin and silica to pastes composed of 5–15 nm sized hydroxyapatite nanoparticles and yielded a bioresorbable composite that is compact, yet flowing upon injection; that prevents setting at room temperature, but sets promptly, in minutes, at 37 °C; that displays an increase in surface porosity following immersion in physiological fluids; that allows for sustained release of antibiotics; and that sets in a tunable manner and in clinically relevant time windows: 1-3 minutes at its fastest. Timelapse, *in situ* X-ray diffraction analysis demonstrated that the setting process is accompanied by an increase in crystallinity of the initially amorphous hydroxyapatite, involving no polymorphic phase transitions in its course. Setting time can be tuned by controlling the weight content of gelatin or powder-to-liquid ratio. The release of vancomycin was slow, ~ 8 % after 2 weeks, and unaffected by the gelatin content. While vancomycin-loaded pastes were effective in reducing the concentration of all bacterial species analyzed, the bacteriostatic effects of the antibiotic-free pastes were pronounced against *S. liquefaciens* and *E. coli*. *S. liquefaciens* bacilli underwent beading and filamentation during the treatment, suggesting that the antimicrobial effects are attributable to cell wall disruption by hydroxyapatite nanoparticles. Vancomycin-loaded pastes augmented the activity of the antibiotic against *P. aeruginosa* and *S. liquefaciens*, while exhibiting no negative effects against human mesenchymal stem cells. They were also uptaken three times more abundantly than pure hydroxyapatite, indicating the theoretical favorability of their use for intracellular delivery of therapeutics. This selectivity, toxic for bacteria and harmless for primary stem cells, is promising for application as bone grafts for osteomyelitis.

Keywords: Antibacterial; Bone graft; Cement; Composite; Hydroxyapatite; Nanoparticles.

1. Introduction

Eight million non-maternal and non-neonatal operating room procedures are performed annually in the US and five out of seven most common ones target the musculoskeletal system[1], the majority of which involve the use of bone grafts to reconstruct hard tissue defects. Despite this,

deficiencies are associated with all the marketable bone substitutes and the search for a bone graft material with ideal physical and biological properties is ongoing[2]. Autologous bone, for one, despite its obvious demerits, still presents the gold standard for bone grafts[3]. However, it necessitates a secondary surgical procedure for its extraction, typically from the donor's iliac crest, fibula or mandibular symphysis. This increases not only the procurement cost and the operative time, but also the chances for postsurgical complications, the patient's discomfort, unaesthetic disfigurements and the overall extraction site morbidity. Bovine derivatives and other xenografts have been used as regular alternatives in the clinic[4], but they increase the risk of infection and immunogenic response and are, like autografts and allografts, subject to variability in composition and properties, leading to significant uncertainties regarding the clinical outcome. Inconsistent osseous incorporation is, thus, a frequent result of autogenous and xenogeneic bone grafting procedures[5]. Moreover, for some localities, particularly the load-bearing ones, such as foot and ankle, systematic metastudies indicate no statistically significant benefit of autografts and other naturally derived grafts over no graft at all[6]. Natural in origin, such grafts also allow for little control over the material properties and their *in situ* adjustment to the bone void location and geometry. Rich in the biomolecular content, biological grafts are also tied to the problem of destructive sterilization, which often contaminates or modifies the material properties in random and unpredictable ways, leading to increased risk of failure[7]. All of this necessitates the quest for viable synthetic alternatives to these biological extracts.

On the physical side, ideal synthetic bone and articular grafts should be moldable in clinically relevant timespans, bind to bone well and have a sufficient mechanical stability, yet degrade with rates that match the new tissue ingrowth, typically ranging from a few weeks to months. On the biological side, ideal synthetic bone and articular grafts, like most biomaterials in general, should possess a sufficient bioactivity and elicit a positive response from the tissue that they come in contact with. To that end, the bone graft should be osteoconductive in terms of being able to attract and induce proliferation of bone cells; osteoinductive in terms of being able to promote the differentiation of osteoprogenitor and pluripotent mesenchymal cells into osteoblasts; and ossointegrative in terms of being able to enter a stable union with the bone tissue that it is being grafted to. The use of hydroxyapatite (HAp) and/or other calcium orthophosphates (CPs) presents a standard approach to endowing a bone graft with sufficient bioactivity and compressive strength[8]. Out of a dozen different CP phases, HAp presents a typical phase of choice because of its being the least soluble[9], the most bioactive[10] and the most mechanically stable[11] of them all, alongside being the natural mineral component of mammalian hard tissues. Pure CP grafts can also be made in a self-setting form, viscous upon the implantation or injection and hardening thereafter[12]. However, the setting timescales of pure CP pastes often extend beyond the ideal therapeutic window that is minutes in range, especially for larger graft volumes[13]. At the same time, pure CP pastes set in relatively dense forms[14,15], extending their resorption rate beyond the optimal range that is a few weeks in duration and offering no control over their porosity[16], which is essential in enabling the bone substitute to mimic the extracellular matrix of bone and provide conditions for infiltration and proliferation of the host cells[17], permeation of the blood plasma and vascularization, thus fostering the osseointegration process.

An immediate advantage of CP grafts is the ability to achieve sustained, locally delivered release of antibiotics into avascular areas that are otherwise inaccessible to systemically administered drugs[18]. However, pure self-setting CP pastes developed in our earlier study[19], albeit offering *in situ* tunable drug release profiles, released antibiotics in the first 2 weeks of immersion in a body fluid. This short duration of the release contrasts the timeline of a typical antibiotic

therapy for chronic osteomyelitis, consisting of 2 weeks of systemic administration on average and being followed by a 6-month course of oral antibiotics[20,21]. To overcome all three of these critical issues, we have introduced gelatin-silica hybrid as an additional component to HAp nanoparticles comprising the pastes developed earlier. The biomimetic choice of HAp and gelatin in the weight ratios ranging from 70 – 77 wt.% and 19 – 26.5 wt.%, respectively, is justified by (a) bone being a composite material, containing approximately 70 wt.% of the mineral, apatite phase, 22 wt.% of collagenous proteins, 5 wt.% of water and 3 wt.% of noncollagenous proteins and other biomolecules[22], and (b) gelatin being collagenous in origin, water-soluble and thus more easily formable into a composite form together with HAp[23] than native collagen[24]. Previous addition of gelatin to porous constructs made of electrospun poly(ε-caprolactone) fibers and supplemented with HAp increased their bioactivity, specifically cell adhesion and proliferation[25]. The combination of methacrylated gelatin and silica also allowed for the fabrication of a porous and photocurable hydrogel with good mechanical and biological properties[26]. By introducing this soft component, we, first of all, attempt to provide a biosoluble constituent that would create pores upon contact with the aqueous medium and be the basis for an injectable tissue engineering construct[27]. Secondly, the role of the additional component is to sustain the release of antibiotics for prolonged periods of time and enable the graft to act either prophylactically or therapeutically, as an antimicrobial bone substitute. And thirdly, the role of this additional component is to shorten the setting timescale from 30 – 45 minutes for relatively large graft geometries down to 2 – 10 minutes, while at the same time decreasing their viscosity and facilitating flow through the syringe during injection. The role of silica as a minor additive was similarly threefold. First, it was to act as a colloidal stabilizer due to silanization[28,29] and, thus, improve the paste flow. Secondly, it was to act as a moderate foaming agent and thus contribute to pore formation. Finally, it was to act as a nucleation agent to further accelerate the setting process initiated by gelation of gelatin at 37 °C and the liberation of the HAp grain surface. In total, the goal of the present study is dual: it is to provide a fundamental insight into the properties and the mechanism of (trans)formation of the material through its precise characterization, but also assess its applicative potentials as a biomaterial through assaying *in vitro*.

2. Materials & Methods

2.1. Synthesis

Aqueous polymer solutions containing either 5 wt.% (composition 1, Table 1) or 7.5 wt.% (composition 2, Table 1) of porcine-skin-derived type A gelatin (*Sigma*) and having the volume of 25 ml were prepared and 25 mg of vancomycin (*M.P. Biomedicals*) were added to them, followed by the addition of 500 μl of tetraethylorthosilicate (TEOS, *Sigma*). In another container, 3 ml of 1 M $NH_4H_2PO_4$ (aq.) (*Fisher Scientific*) were added dropwise to 2.5 ml of 2 M $Ca(NO_3)_2$ (aq.) (*Fisher Scientific*), followed first by the addition of 9 ml of concentrated, 28 % NH_4OH (*Sigma Aldrich*) to raise the pH and then by the addition of 85 ml of deionized, Millipore water. The resulting milky suspension containing HAp nanoparticles was stirred with the magnetic bar and brought to boil, at which point it was poured into the polymer solution while stirring at 400 rpm. The colloidal mixture then had 5 ml of 3 mg/ml aqueous solution of vancomycin added to it while stirring. The colloid was sedimented by centrifugation and washed with deionized water. The resulting precipitate was dried overnight in vacuum (- 25 mmHg, Savant SPD1010 Speedvac concentrator). Unless otherwise noted, the dried composite powders crushed in a mortar down to

fine particle size were mixed with a liquid phase in 0.33 mg/µl powder-to-liquid (P/L) ratio to yield the paste-like formulations. An aqueous solution of NaH_2PO_4 (2 wt.%, *Fisher Scientific*) was used as the liquid phase unless otherwise noted. The manual mixing proceeded by adding the powder gradually to the liquid phase while stirring with a spatula so as to preserve the formulation in the pasty state. Following the mixing of the solid and the liquid phase, the paste was vortex-mixed in 1.5 ml Eppendorf tubes for 5 min at 2000 rpm, then poured onto a plastic Petri dish and allowed to set at either 25 ^{o}C or 37 ^{o}C. Vortex-mixing was performed in almost full Eppendorf tubes to minimize the exposure to air and the dissipation of the paste on the tube walls. The simplified schematics of the synthesis protocol is shown in Fig.1. Assuming that the precipitation, condensation and capture of HAp/gelatin, silica and vancomycin, respectively, were complete, the estimated two composite paste compositions, whose precursors differed only in the abovementioned amount of gelatin (5 and 7.5 wt.% in the precursor gelatin solution), are listed in Table 1. Table 2 lists the vancomycin loading efficiency in the two compositionally different pastes. Per Eq.1, the loading efficiency (LE), equivalent to the weight percentage of vancomycin in the final composition, was measured by normalizing the weight of the encapsulated drug (m_d) to the total weight of the carrier (m_c). The drug content (m_d) was determined by measuring the absorbance on a UV/Vis spectrophotometer (Nanodrop 2000, Thermo Scientific) at $\lambda = 200$ nm.

$$LE = m_d/m_c \text{ x } 100 \text{ (\%)} \qquad\qquad (Eq.1)$$

Table 1. The two composite paste compositions analyzed, differing most critically in their weight contents of gelatin: 19.4 and 26.5 wt.%.

Composition	HAp (wt.%)	Gelatin (wt.%)	Silica (wt.%)
1	77.4	19.4	3.2
2	70.5	26.5	3.0

Table 2. Vancomycin loading efficiency for the two types of composite pastes.

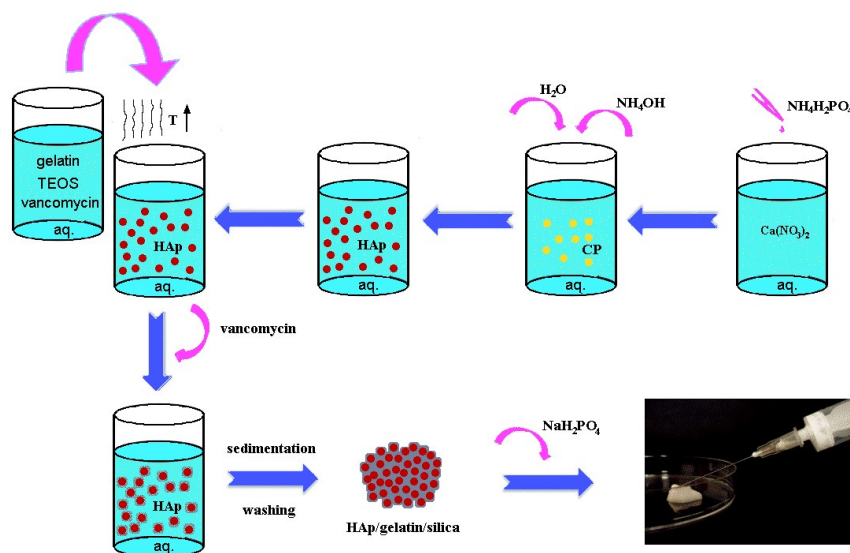| Composition	Loading efficiency (wt.%)
1	10
2	8.8

Fig.1. Schematic representation of the major steps in the synthesis of the self-setting HAp/gelatin/silica composite paste.

2.2. Physicochemical characterization

Scanning electron microscopy (SEM) studies were carried out on a JEOL JSM 6320F-FESEM operated at 3.2 kV voltage and 8 μA beam current. Sample preparation involved depositing powders or pastes on clean aluminum stubs using the carbon tape and sputter-coating them with gold to reduce the surface charging effects. X-Ray diffraction (XRD) studies were carried out on a Bruker D2 Phaser diffractometer using polychromatic Cu as the irradiation source. K_β line was stripped off with an inbuilt filter, whereas $K_{\alpha 2}$ line was stripped off manually. The step size and the irradiation time per step were 0.01 ^{o} and 1 second for the regular measurements and 0.02 ^{o} and 0.3 seconds for the timelapse ones. Particle size distribution of the composite HAp-gelatin-silica pastes dispersed in water was analyzed using a Malvern Zetasizer dynamic light scattering analyzer. Transmission electron microscopy (TEM) studies were performed on a JEOL JEM 1220 Life Science TEM operated at 80 kV.

2.3. Setting time determination

To determine the setting time variations based on the polymer content in the composite pastes, two different gelatin concentrations (19.4 wt.% and 26.5 wt.%) were used to synthesize the pastes. The setting time of the samples was divided to two categories: the initial setting time and the final setting time. The measurements were done in accordance with ISO 1566. The standard Vicat needle method (ASTM C191-92) was used on samples placed in 47 mm plastic Petri dishes (*Fisherbrand*) and incubated at 37 ^{o}C. The sample was considered initially set when the needle (30G hypodermic disposable needle, *EXEL International*) made a slight circular indentation on the surface of the sample, but was far from the bottom. The final setting time was noted when the needle failed to make any visible indentation on the sample surface.

2.4. Drug release assay

Vancomycin-loaded pastes were allowed to completely set before they were placed in 50 ml of phosphate buffered saline (PBS) in closed conical tubes and incubated at 37 °C and 50 rpm rotation perpendicular to the cylinder axis. The drug release rates were determined in duplicates by taking 1 ml PBS on daily basis for two weeks. The volume of the aliquoted solution was replaced each time with fresh PBS. The drug content was determined spectrophotometrically, as described in Section 2.1.

2.5. Antibacterial assay

In the liquid inoculation test of the vancomycin-containing samples, a single colony of *Staphylococcus aureus* cultured on a blood agar plate over a period of 24 h was stabbed with a pipette tip and placed in 5 ml of brain heart infusion broth (*Sigma Life Sciences*) and incubated overnight at 37°C and 170 rpm. The same procedure was repeated for *Escherichia coli*, *Serratia liquefaciens*, *Salmonella entiritidis*, and *Pseudomonas aeruginosa*, all of which were cultured on nutrient agar plates and inoculated in the nutrient broth (*Sigma Life Sciences*). Twenty-five microliters of pastes were added to the infected broths. All the samples were analyzed in duplicates. Antibiotic-loaded pastes were compared against sets of three controls: one negative control contained 5 ml of the broth in which a single colony of a bacterium was introduced and then incubated for 24 h; the second negative control had the pastes containing no antibiotic added to the bacterially infected broth in order to determine the antibacterial efficacy of the sole paste; the positive control had the antibiotic added to the bacterially infected broth in the same amount as that contained in the 25 µl of the paste, i.e., 2.5 mg for the 19.4 wt.% gelatin-containing paste and 2.2 mg for the 26.5 wt.% gelatin-containing paste. Staining of bacteria with crystal violet and safranin was performed with a gram-staining kit (*Sigma-Aldrich*) applied on glass slides following an overnight treatment with the composite pastes.

2.6. hMSC viability assay

A 12 mM 3-[4, 5-dimethylthiazol-2-yl]-2,5-diphenyl tetrazolium bromide (MTT) stock solution was prepared by adding 1 ml of sterile PBS to a 5 mg vial of MTT and vortex-mixing to ensure complete dissolution. Earlier, human mesenchymal stem cells (hMSCs, courtesy of Anne George, University of Illinois at Chicago) were seeded at the concentration of 5×10^3 cells/well in a 96-well plate and 2 μl of the composite HAp pastes were added to each well. The cells were incubated with the pastes for 24 hours in 100 μl of the general hMSC culture medium without ascorbic acid (StemPro MSC SFM) and 10 wt.% fetal bovine serum (FBS). After the given incubation period, the culture media were replaced by 100 μl of the fresh media of the same composition. Then, 10 μl of the 12 mM MTT stock solution were added to each well containing the pastes as well as to the control wells. This was followed by incubation at 37 °C for 4 hours. Subsequently, the cell culture medium in each well was removed until 25 μl/well remained. Then, 50 μl of dimethyl sulfoxide (DMSO) was added to each well and mixed in with a pipette tip. The well plate was incubated again at 37 °C for 10 minutes, after which the samples were mixed again and absorbance values were measured at $\lambda = 540$ nm. The positive control consisted of the cells with the growth medium, while the negative control contained only the growth medium without the cells. All the samples, including the controls, were analyzed in triplicates and their absorbance values were normalized to the absorbance of the negative control.

2.7. Immunofluorescent analysis

hMSc grown on glass coverslips in 24-well plates in the general hMSC culture medium with 10 wt.% FBS were treated with 5 mg/ml of either HAp or HAp-gelatin-silica paste and incubated for 24 h. The cells washed with PBS and fixed for 5 minutes in 4% paraformaldehyde, before being rewashed with PBS and incubated with Alexa Fluor 568 Phalloidin (1:400) (*Molecular Probes*) and OsteoImage[TM] bone mineralization staining agent (*Lonza*) for 30 minutes. Cells were then washed 3 times with PBS and cell nuclei were counterstained using NucBlue fixed cell ReadyProbe reagent (*Molecular Probes*) for 20 minutes. Images were obtained using a Nikon T1-S/L100 inverted epifluorescent confocal microscope. All the samples were analyzed in duplicates.

3. Results and discussion

The pastes were composed of uniformly dispersed, ultrafine HAp nanoparticles with sizes in the 5 – 15 nm range (Fig.2a). The narrowness of this primary particle size distribution is seen from the histograms obtained from SEM measurements (Fig.3a). The confinement of these primary particles inside the polymeric matrix increases the hydrodynamic particle size up to ~ 200 nm (Fig.3b). TEM imaging was used to visualize the polymeric matrix enveloping the nanoparticles inside larger units (Fig.2b). Zeta potential (ζ) of the colloidal suspensions of particles in water as the function of pH is shown in Fig.4. The ±15 mV is typically considered the threshold for colloidal stability[30], yet for both HAp and HAp-gelatin-silica particles, the zeta potential was found in the $- 20 < \zeta < 15$ mV range, indicating little to no conditions for colloidal stability except in the pronounced acidic range, at pH < 3, where the dissolution of HAp is copious, if not complete. Zeta potential of pure HAp in water was particularly low under physiological conditions, < 5 mV, suggesting the strong propensity for aggregation. This propensity became lowered following the addition of the negatively charged gelatin and silica. As a result, zeta potential in the physiological pH range was pushed towards more negative values, specifically from 3.27 mV for pure HAp to – 0.06 mV for the HAp composite containing 19.4 wt.% gelatin to – 7.48 mV for the HAp composite containing 26.5 wt.% gelatin. The points of zero charge correspondingly decreased following the addition of gelatin-silica to HAp (Fig.4).
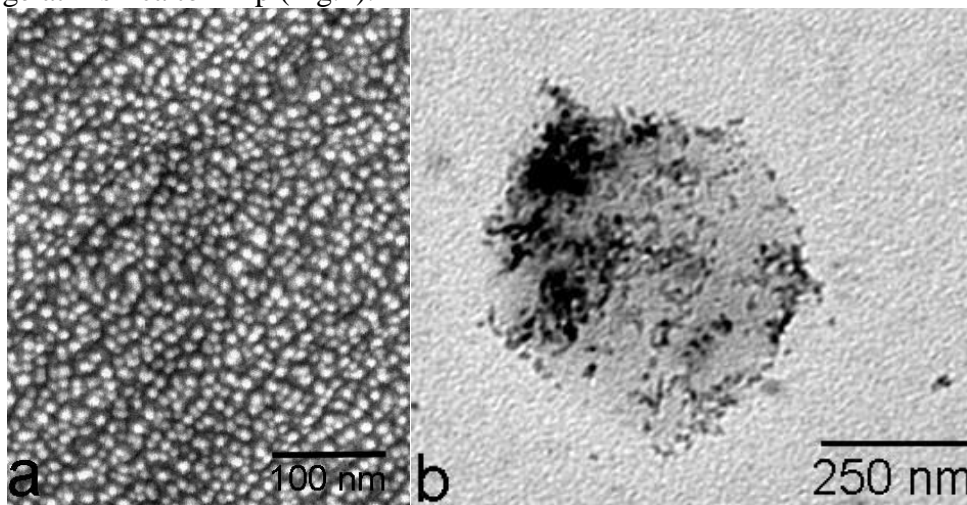

Fig.2. SEM (a) and TEM (b) image of set HAp-gelatin-silica pastes showing the presence of HAp nanoparticles (a) and their encapsulation within an amorphous, polymeric gelatin/silica shell (b).
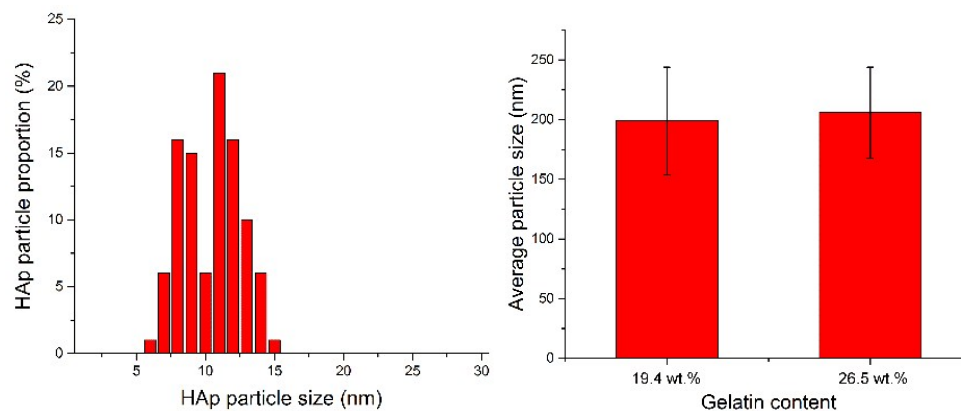
Fig.3. SEM-derived particle size distribution histogram for HAp nanoparticles comprising the composite HAp-gelatin-silica pastes (a) and DLS-derived average particle size of the composite HAp-gelatin-silica pastes with two different gelatin contents, 19.4 and 26.5 wt.%, suspended in water (b). Data are shown as averages with error bars representing standard deviation.
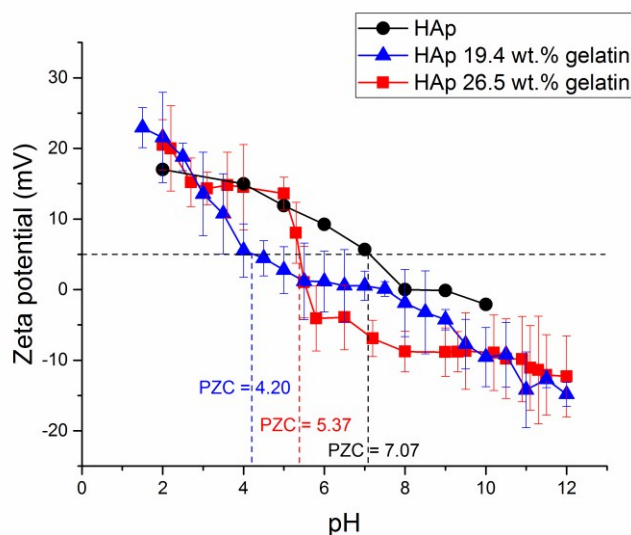

Fig.4. Zeta potential vs. pH curves for HAp nanoparticles comprising the composite HAp-gelatin-silica pastes and for the composite HAp-gelatin-silica pastes containing 19.4 and 26.5 wt.% of gelatin. Points of zero charge (PZC) are denoted in the graph. Data are shown as averages with error bars representing standard deviation.

The fresh pastes prepared *in situ* by mixing the solid and the liquid component set in clinically ideal timespans. The pastes can be mixed in powder-to-liquid (P/L) ratios to allow for setting times ranging from 1 to 20 minutes for the initial setting times and from 3 to 25 minutes for the final setting times (Fig.5a-b). These times show direct dependence on the weight content of the gelatin component of the paste. As the gelatin content at P/L = 0.33 mg/μl increases from 19.4 to 26.5 wt.%, so does the initial setting time increase from 2.3 to 3.6 minutes and the final setting time from 5 to 8 minutes (Fig.5a). As in partial agreement with a previous report[31], gelatin added to CP pastes shortens the span between the initial and the final setting time. At the same time, the P/L ratio demonstrates an inverse proportionality to the setting times (Fig.5b). As it increases from 0.1 to 0.5 mg/μl, the initial setting times drop from 20 to 1 minute and the final

setting times drop from 25 to 3 minutes. Below this range the pastes are too dilute to allow for the close particle-particle contact and the entwinement of the growing HAp crystals in the setting stage. Since this is what defines the solidity of the hardened paste, excessively low P/L ratios (< 0.1 mg/μl in this case) directly translate to insufficient cohesiveness of the final product. Above the given range (> 0.5 mg/μl) the grains comprising the paste are deprived of proper perfusion of the liquid activator of the setting process, as the result of which no pervasive grain binding can occur and the cohesiveness equally suffers. Within the range outlined in Fig.5b, 0.1 mg/μl < P/L < 0.5 mg/μl, higher P/L ratios and shorter setting times coincide with greater cohesiveness and geometric integrity of the final product. As a result, the less viscous pastes set slower, but are injectable through smaller diameter hypodermic needles, coinciding with larger gauge numbers. As seen from Fig.5b, all pastes are fully drawable into the syringe and extrudable using G20-24 hypodermic needles, although thicker pastes required lower G numbers. Pastes in the low G range are moldable, but less prone to injection without causing the phase separation due to pressure gradient issues. The setting reaction is, however, expected to be subject to minor variations depending on the volume and the geometry of the paste. Lower volumes and geometries with higher exposed surface area will, for example, set somewhat faster than their opposites, and the difference can be as high as ± 50 % of the temporal values denoted in Fig.5b.

Bone is an organ whose functionally gradient structure displays a large variability between the surface and the interior. For example, the cortical surface of long bones possesses a markedly lower remodeling rate and porosity than the cancellous bone lying closer to the marrow[32]. This poses the demand for grafts with tunable setting rates and the ability to match the local tissue turnover and the vascular flux[33]. On top of this, the idea that zero-order release kinetics is ideal for each drug delivery application has become obsolete and is gradually ceding place to the concept of chronopharmacokinetics as the systematic adjustment of the release profiles to circadian and other rhythmic flows of metabolites present in the target area[34]. Here we see that the setting times of the HAp-gelatin-silica composite pastes can be tuned by controlling their gelatin content (Fig.5a) and by controlling their P/L ratios (Fig.5b). As for the latter, an exponential, first-order kinetics is associated with this effect and the linear fit of the logarithmic dependence of the final setting time on P/L ratio gives a good correlation coefficient value ($R^2 = 0.93$, Fig.5c), allowing also for the calculation of the final setting time in minutes, t, for a given P/L ratio in mg/μg using the following empirically derived equation:

$$t = 10^{1.33 - 1.712(P/L)} \qquad (0.1 \text{ mg/μl} \leq P/L \leq 0.5 \text{ mg/μl})$$

The phenomenon of directly proportional increase in the weight content of gelatin and the duration of the setting reaction is the consequence of the fact that the phase transformation from amorphous CP to crystalline HAp, governing the setting process, proceeds partially by following the surface dissolution/reprecipitation mechanism. For this reason, for example, the timely imposition of a solid polymeric coating around the freshly precipitated CP nanoparticles has the ability to hamper their phase transition into a more crystalline and thermodynamically stable state, freezing their structure in a comparatively amorphous and more active state[35]. The same effect is at play here: gelatin-silica component partially blocks the CP particle contact and the surface diffusion of CP ionic growth units (Ca^{2+}, PO_4^{3-}, OH^-), slowing down the crystallization process as the result. Since a very small amount of gelatin is sufficient to block the particle surface and gelatin does not set at 37 °C, any further increase in its content slows down the setting process, as demonstrated by Fig.5a.

This brings us over to perhaps the most interesting effect achieved by adding gelatin to HAp: immobilized setting reaction at room temperature. A comparison between the setting times at 25 and 37 °C is shown in Fig.5d, demonstrating that the pastes could be prepared *in situ* in a clinical setting without concern that they might prematurely set. Implanted, however, and introduced into a 37 °C environment, the setting reaction is activated and proceeds at clinically ideal timespans, i.e., in a couple of minutes. Thus, for a composite HAp paste containing 19.4 wt.% gelatin and mixed with 2 wt.% NaH_2PO_4 in 0.5 mg/μg P/L ratio, the initial and the final setting reactions end after 39 and 53 minutes, respectively, at room temperature, as opposed to only 1 and 3 minutes at the physiological temperature (Fig.5c). As mentioned, solid gelatin coating around CP nanoparticles retards the setting reaction that proceeds by following the dissolution/recrystallization mechanism. However, gelatin undergoes gelation at 37 °C, disentangling from CP grains and liberating their surface, thus effectively activating the setting reaction.

To explain the faster setting of gelatin-containing pastes compared to pure HAp ones, a catalytic role must be ascribed to gelatin. One possibility is that gelatin contributes with active groups that serve as nucleation centers, accelerating the crystallization process that governs the setting reaction. The minor presence of silica and/or silylation of gelatin prior to its admixing to CP sol are supposed to augment the nucleation promotion capacity of gelatin alone and, together with the effect of Si-O-Si polymerization[36,37], speed up the setting reaction. The other possibility is that gelatin as gel buffers the setting reaction by consuming the chemical potential imparted by the liquid phase, accelerating the reaction as the result, but making it less complete, the evidence of which may be the lower compressive strength of gelatin-containing HAp pastes compared to the pure HAp ones. If this is correct, then gelatin, counterintuitively, plays a role antipodal to that of a binder. In any case, the effect of gelatin on the setting reaction is apparently twofold. At low concentrations, it speeds it up. Thus, at identical P/L ratios, the setting times are 7 – 8 times lower when gelatin (19.4 wt.%) is added to the paste composition. At higher concentrations, however, being a passive component from the hardening process standpoint, it slackens it by interfering with dissolution/recrystallization intrinsic to the setting reaction. This is evidenced by the increased setting time when the concentration of gelatin in HAp pastes is increased by approximately one quarter, i.e., from 19.4 to 26.5 wt.% (Fig.5a).
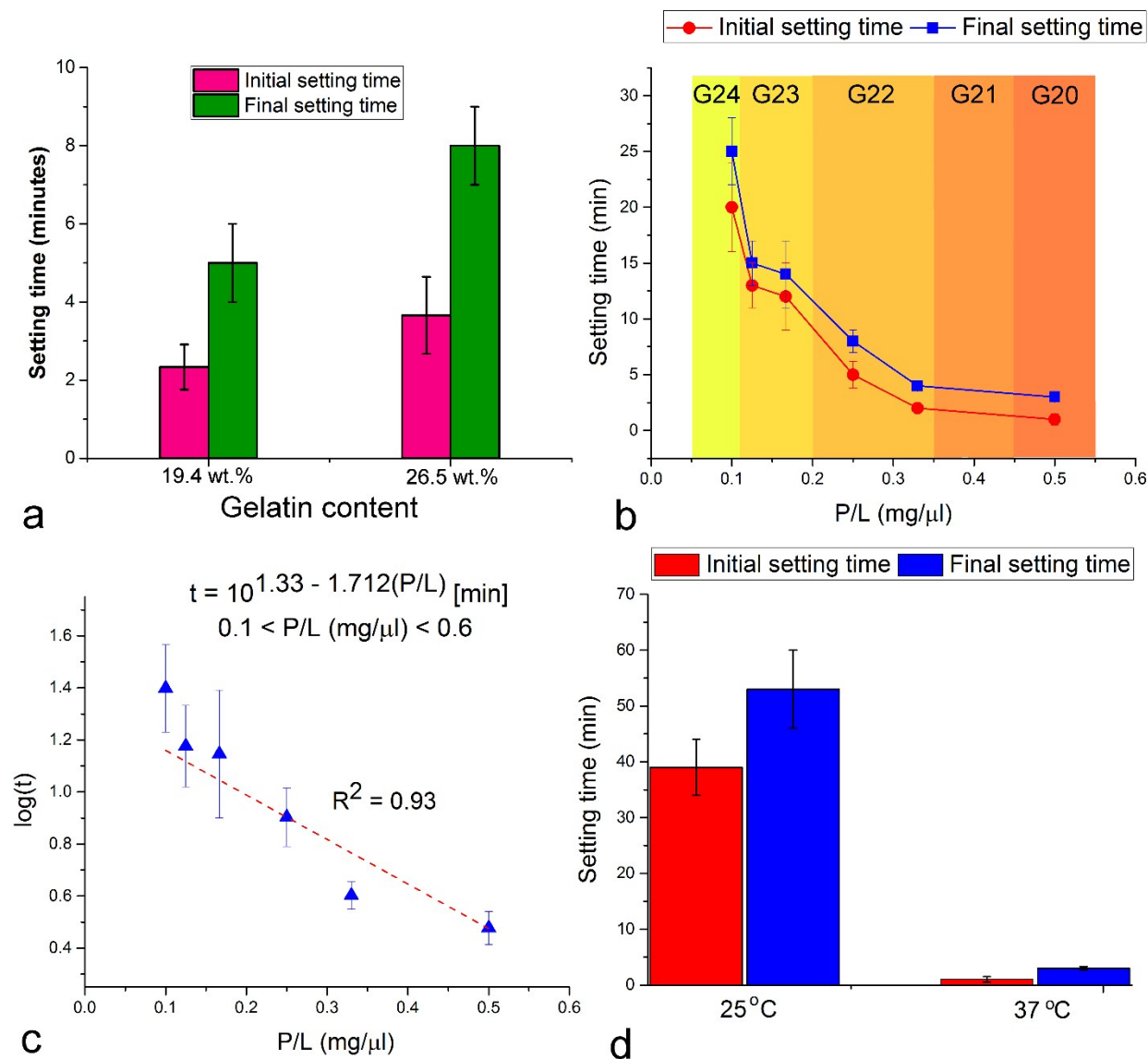
Fig.5. (a) Variation of the initial and the final setting times of HAp-gelatin-silica composite pastes depending on: (a) the content of gelatin in pastes with powder-to-liquid ratio (P/L) of 0.33 set at 37 °C using 2 wt.% NaH_2PO_4 as the liquid phase; (b) P/L ratio in 60 μl 19.4 wt.% gelatin-containing pastes set at 37 °C and 2 wt.% NaH_2PO_4 as the liquid phase, along with the maximal hypodermic needle gauge numbers capable of extruding the paste in air for the given P/L ratio ranges (b), the setting temperature of 60 μl 19.4 wt.% gelatin-containing paste with P/L = 0.5. The logarithmic plot of the final setting time (minutes as units) of 19.4 wt.% gelatin-containing pastes in (b) as a function of P/L ratio is shown in (c), along with the linear fit, the R^2 value and the equation derived to correlate the setting time at 37 °C with the P/L ratio. Data are shown as averages with error bars representing standard deviation.

The integrity and setting kinetics of the pastes differed depending on the chemical identity and concentration of ions comprising the aqueous liquid phase. Thus, substituting Na^+ with K^+ speeds up the setting process, which is expected by knowing that Na^+ is a more effective substituent of Ca^{2+} in HAp than K^{+}[38] and, thus, a more potent inhibitor of its crystallization[39,40,41], the process intrinsic to the setting reaction. In turn, K^+ solutions yield crumblier solids than Na^+ ones, which can be explained by the fact that, although K^+ and Na^+ neighbor each other in the Hofmeister series[42], K^+ is a less hydrated ion, meaning that its presence in the interfacial layer

might interfere with the growing crystal entwinement by increasing the surface tension and lowering the entropy of the hydration sphere compared to the effect exhibited by Na^+. The combination of the two ions in the liquid phase can partially make up for the weaknesses of both of them alone, although the properties of the final product turn out to be highly dependent on Na^+/K^+ molar ratios. Increasing the concentration of NaH_2PO_4 from 2 to 5 wt.% lowers the brittleness and produces more viscous pastes which also set negligibly faster, whereas the same change in the concentration for KH_2PO_4 increases the setting time, but produces no significant change in mechanical integrity. The addition of vancomycin did not interfere significantly with the setting reaction kinetics. Immersion of the set HAp composite paste containing 19.4 wt.% gelatin in water for three weeks leads to partial degradation of the smooth and nonporous surface of the hardened paste and dissolution of the water-soluble gelatin component, thus creating indents and macropores (i.e., pores larger than 50 nm per IUPAC notation), the size of some of which is sufficient to accommodate cells (Fig.6). The connection between the pores is, however, absent, presenting a critical obstacle to the uninterrupted flux of nutrients and waste products in and out of the structure and thus to the long-term internal population of the material with the cells. Preventing the collapse of the hard, HAp component following the escape of the soft, gelatin component is a challenge that needs to be solved before these pastes can be used as injectable ceramic scaffolds. After three weeks of immersion, the set pastes visibly crack and dissipate, thus fulfilling the requirement necessary to enable the substitution of the graft by the naturally ingrown bone tissue over the typical period of three weeks. A direct correlation between porosity and pore-forming ability of CP implants and their degradation and resorption rates was previously established[43,44]. Also, as seen from Fig.6, pastes set with K^+ ions in the liquid phase are more dissipative, preserving shape to a lesser extent than pastes set in the presence of Na^+.
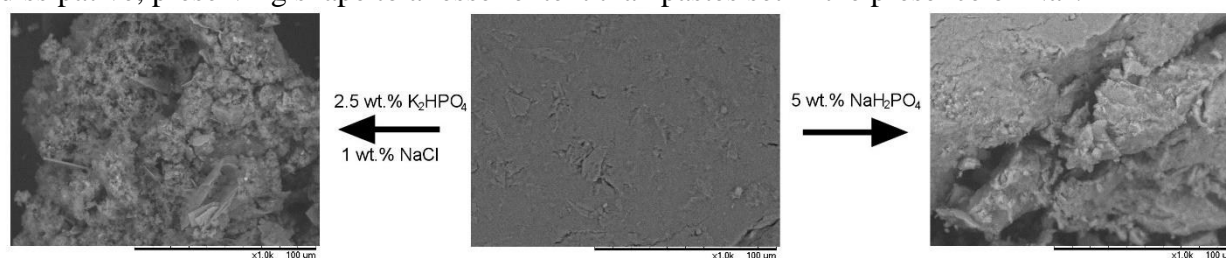

Fig.6. SEM images of a set HAp-gelatin-silica composite paste prior (center) and after three weeks of incubation in water (left and right), differing only in the liquid phase used in the paste formation stage: 2.5 wt.% K_2HPO_4 and 1 wt.% NaCl (left) or 5 wt.% NaH_2PO_4 (right).

Fig.7 displays a difference in the X-ray diffractograms of a composite paste and of its two major individual components, HAp (70.5 – 77.4 wt.%) and gelatin (19.4 – 26.5 wt.%). Gelatin is detected in the precursor powder as an amorphous hump peaking at $2\theta = 20$ ° - 22 °. However, neither of the two amorphous components, gelatin and silica, were detected in the XRD patterns of the composite. Dry gelatin exhibited some level of crystallinity, which is being lost following its reconstitution and mixing in with the HAp powder. Since HAp nanoparticles are precipitated prior to their mixing with the organic and silica components, no significant change in the crystallinity of the inorganic phase was observed. Fig.8 shows the changes in crystallinity of the inorganic HAp phase throughout the first two hours following the onset of the setting reaction. These timelapse XRD measurements evidenced that the setting process was accompanied only by an increase in the crystallinity of the initially poorly crystalline HAp and not by a transformation in the phase composition. Thus, only the most intense, (211) reflection of the hexagonal $P6_{3/m}$ HAp lattice is seen in the $30 – 41$ ° 2θ range for the paste at time zero, immediately after the mixing of

the solid and the liquid phase, as well as in the patterns taken during the following 8 minutes. Only at the 10th minute does the noise due to amorphousness begin to subside and the (300) reflection appears as a shoulder of the (211) reflection at 32.90 º as well as the (310) reflection at 39.86 º. This is in accordance with our previous data on similar systems, showing that the setting of this type of pastes is rare in a sense that it neither involves one of dicalcium phosphates, typically brushite, as the end product nor does it involve tri-/tetra-calcium phosphates as precursors. Rather, it is accompanied solely by a change in crystallinity. The setting reaction of the sample analyzed using timelapse XRD was over in 15 minutes and this was reflected in the settling of the crystallinity (Fig.8). An obvious increase in the absolute intensities (Fig.8a) as well as a reduction in the background noise (Fig.8b) coincided with the detection of the final setting point. The fact that no detectable changes in crystallinity were detected during the first 10 minutes of the setting process suggests an autocatalytic route. The analysis of patterns in-between the initial and the final setting time, i.e., in the 10 – 30 minute time range, indicated a finite degree oscillatory changes in crystallinity (Fig.S1). Such oscillations between different equilibrium states in a liquid-to-solid phase transition were previously noticed and attributed in origin to diffusive fluxes at the interface between phases[45]. Oscillations were also observed at the particle-solution interface during precipitation and dissolution reactions and were correlated with autocatalysis or reaction inhibition by the product formation[46]. In the absence of a constant influx of the driving energy for the amorphous-to-crystalline transition and back, the oscillatory reaction eventually settles in an equilibrium state[47]. Synchronization enabled by the local variations in the chemical potential[48] due to competing crystallization and dissolution reactions is responsible for sustaining the nonlinear, oscillatory dynamics at the solid/liquid interface and can be tied to pattern formation, indirectly explaining the co-evolution of CP and the higher organisms. Here it is worth noting that the transformations in the solid phase entailing the setting process and involving changes in crystallinity exceed in duration the time length of the mechanical aspect of the setting process and that the thermal energy under ambient conditions continues to stabilize the crystalline phase over time. As a result, prolonged storage of the precursor powder can hinder the cement formation process by blocking the temporary restoration of the amorphous phase on which this process depends.
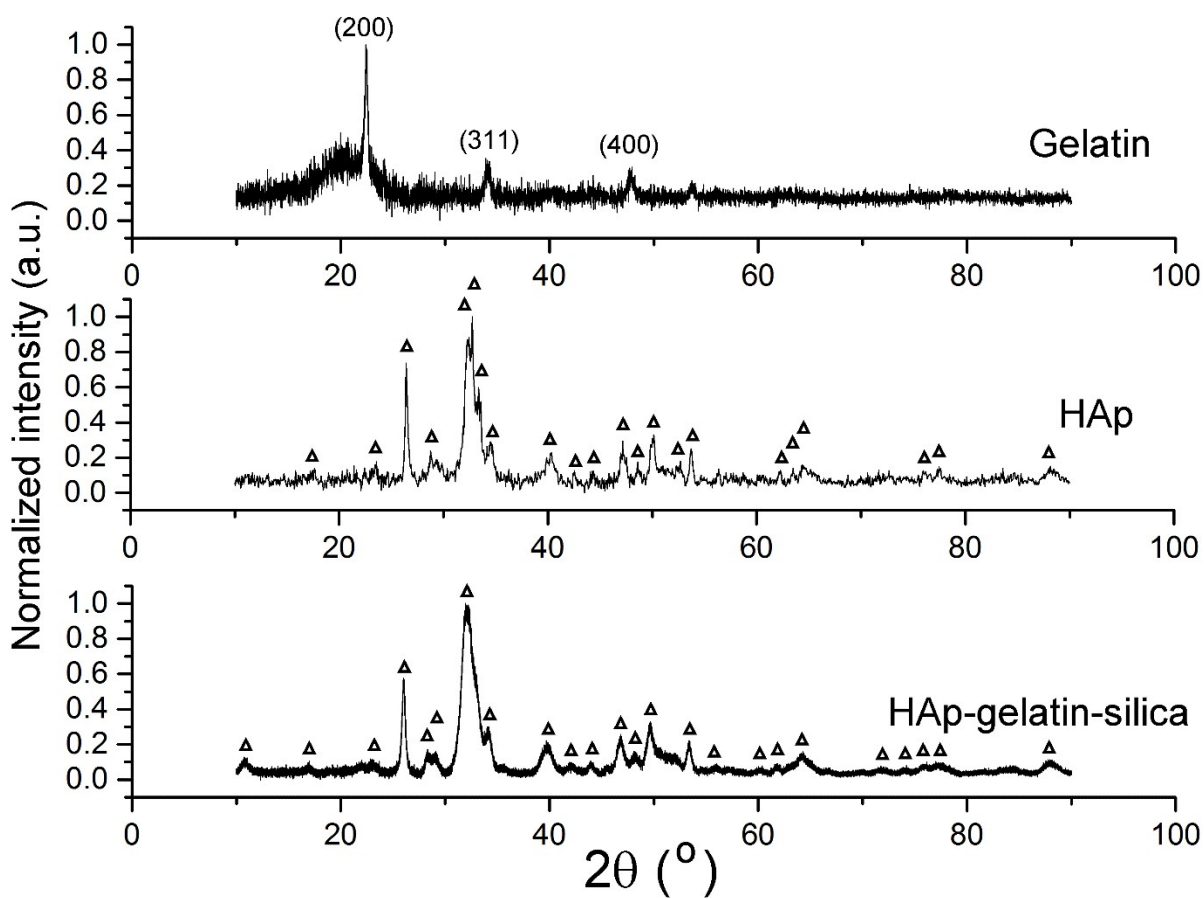
Fig.7. XRD patterns of a composite HAp-gelatin-silica paste and of its major two individual components: HAp and gelatin. Reflections derived from HAp are marked with Δ.
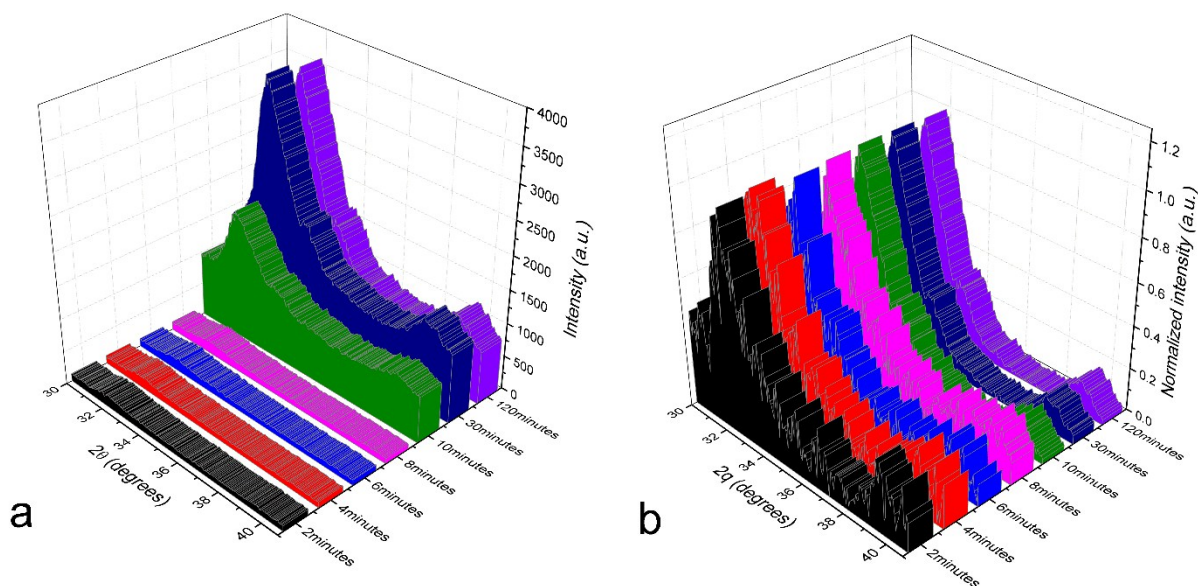
Fig.8. Timelapse XRD patterns of the composite, vancomycin-loaded HAp-gelatin-silica pastes containing 26.5 wt.% of gelatin in the course of the setting process taking 15 minutes to reach the final setting time. Patterns were taken in the course of 120 min following the initiation of the setting reaction and are plotted with both absolute (a) and relative (b) diffraction intensities.
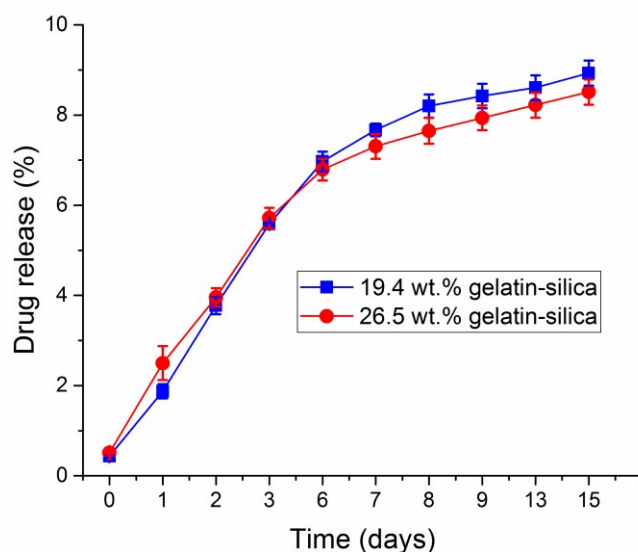

Fig.9. Vancomycin release profiles of HAp-gelatin-silica pastes containing different amounts of the gelatin component: 19.4 and 26.5 wt.%. The last two data points for the 26.5 wt.% gelatin system are the result of extrapolation of the preceding portion of the curve. Data are shown as averages with error bars representing standard deviation.

Unlike the setting time, tunable as a function of the gelatin content (Fig.5a) or the P/L ratio (Fig.5b-c), the rate of release of vancomycin from the pastes immersed in SBF showed no dependence on the weight ratio of gelatin in the composite (Fig.9). In our previous study, we demonstrated that the weight ratio between two HAp components in a self-setting paste can be used to tune both the setting rate and the rate of release of different antibiotics. In this study we see no effect of the variation of the weight proportion between the two major components of the

paste, HAp and gelatin, on the release kinetics. Still, for both composite pastes analyzed (Fig.9), the release is slower and more sustained than that achieved from pure HAp pastes. Extrapolation of the release profiles toward the data point of complete, 100 % release suggests that it would take approximately a year for the release of vancomycin to reach completion. The fact that the drug release kinetics is independent on the content of gelatin suggests that the release is controlled through the affinity of vancomycin for HAp. In other words, vancomycin is expected to bind primarily to the surface of HAp through electrostatic attraction and be released by overcoming this attraction with the help of the hydration force. The parallel increase in vancomycin loading efficiency and the weight percentage of HAp in the paste (Tables 1 and 2), by the same factor of 1.1, supports the idea that vancomycin predominantly gets adsorbed onto HAp instead of being entrapped by gelatin. Still, by coating HAp grains and hindering the desorption of the drug, gelatin allows for its slower and more sustained release. With the first week of release yielding a linear, concentration-independent, zero-order profile and showing no signs of burst release, there is a concern that this type of release may not exceed the minimal inhibitory concentration (MIC) and will favor the rise of resistance to the antibiotic therapy among the pathogens. On one hand, to deepen this question, we performed the antibacterial testing of the composite pastes *in vitro*. On the other hand, with the release totaling ~ 2 % of the total drug content in the first 24 h, equaling 2 mg/g of the paste, it would take only 1 g/dm^3 of the paste to reach the uppermost end of the MIC for vancomycin against methicillin-resistant *S. aureus* (2 μg/ml)[49] in this period of time. Such an absence of the burst release indicates that the antibiotic is almost completely confined to the interior of the hardened paste and that the degradation of the paste in an aqueous environment will precondition its antibacterial activity. Although it is probable that a small amount of antibiotic will settle on the surface of the paste upon its setting, it is also hardly conceivable that this amount would be sufficient to cause an antibacterial effect that is markedly microbicidal and not purely prophylactic.
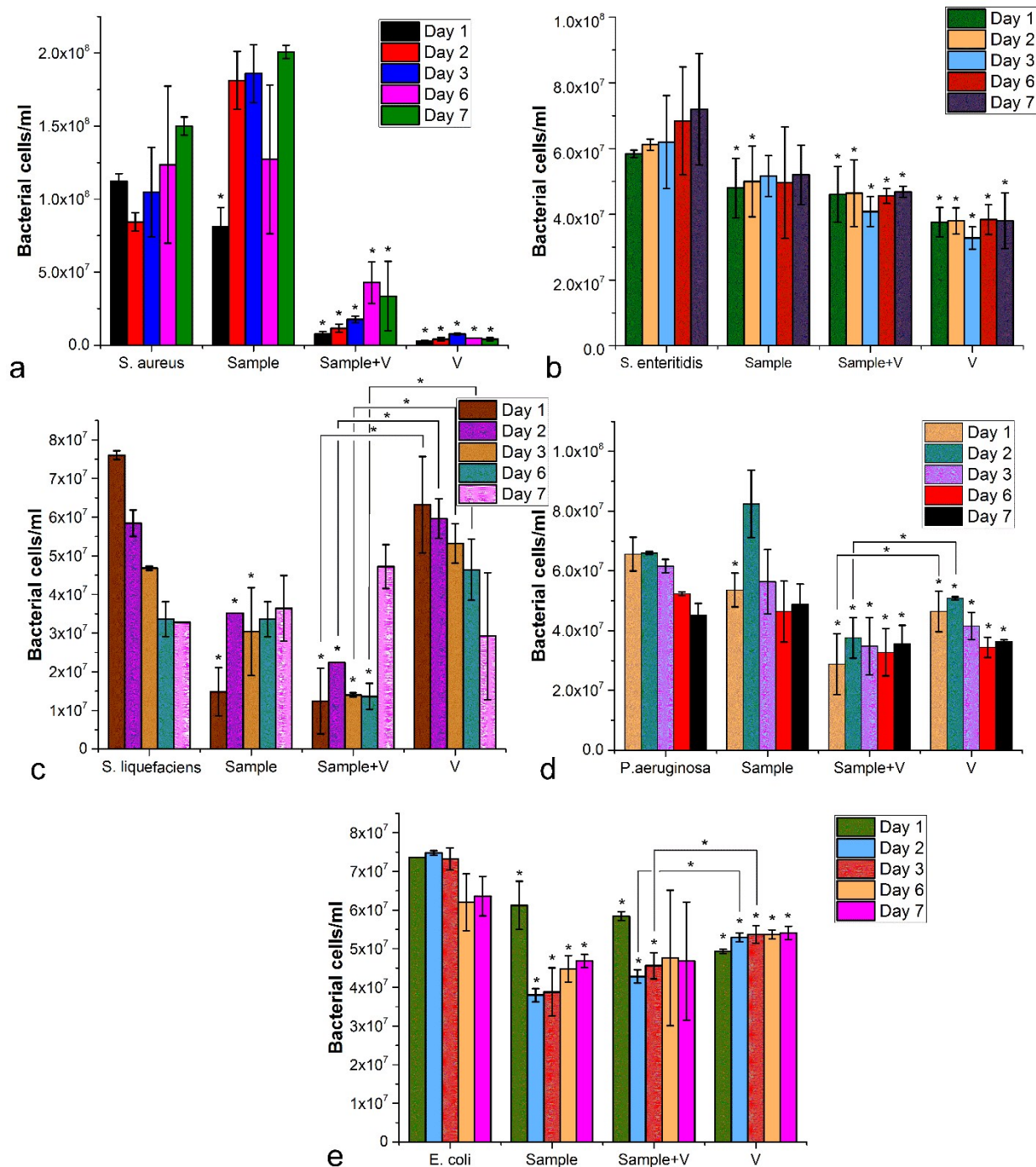
Fig.10. Bacterial population in a liquid inoculation assay of vancomycin-free composite HAp pastes containing 19.4 wt.% gelatin (Sample), vancomycin-loaded composite HAp pastes containing 19.4 wt.% gelatin (Sample + V) and pure vancomycin (V) against (a) *S. aureus,* (b) *S. enteritidis,* (c) *S. liquefaciens,* (d) *P. aeruginosa* and (e) *E. coli.* Assays were carried out after days 1, 2, 3, 6 and 7. Data are shown as averages with error bars representing standard deviation. Data points significantly lower in value compared to the untreated control (far left, $p < 0.05$) are topped with an asterisk. Asterisks topping the lines connecting individual data points from the Sample + V group with the corresponding data points from the V group denote the significantly lower ($p < 0.05$) values in the former group compared to the latter.
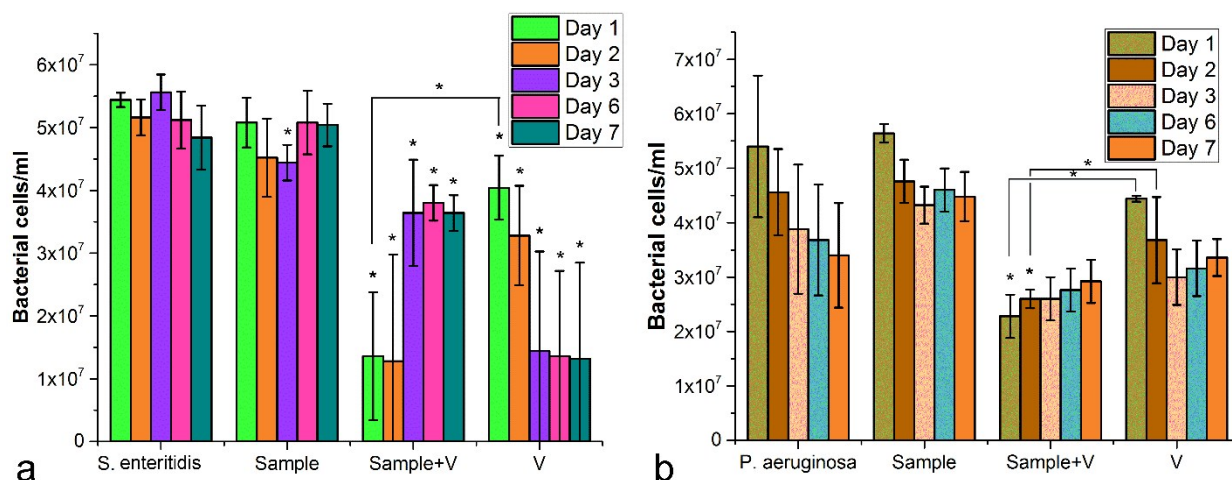
Fig.11. Bacterial population in a liquid inoculation assay of vancomycin-free HAp pastes containing 26.5 wt.% gelatin (Sample), vancomycin-loaded composite HAp pastes containing 26.5 wt.% gelatin (Sample + V) and pure vancomycin (V) against (a) *S. enteritidis,* and (b) *P. aeruginosa.* Assays were carried out after days 1, 2, 3, 6 and 7. Data are shown as averages with error bars representing standard deviation. Data points significantly lower in value compared to the untreated control (far left, $p < 0.05$) are topped with an asterisk. Asterisks topping the lines connecting individual data points from the Sample + V group with the corresponding data points from the V group denote the significantly lower ($p < 0.05$) values in the former group compared to the latter.

Nanostructured drug delivery carriers are known for their ability to enhance the antibiotic therapies[50] and their role is expected to be especially prominent against intracellular pathogens[51]. Vancomycin-loaded composite pastes were effective in reducing the concentration of all five types of bacteria analyzed in this study: *S. aureus, S. enteritidis, S. liquefaciens, P. aeruginosa,* and *E.coli*. Still, there was a notable difference in the activity: it was more pronounced against *S. aureus*, *S. liquefaciens* and *P. aeruginosa* than against *E. coli* or *S. enteritidis*. The antibiotic-loaded pastes were also more effective than the pure, antibiotic-free pastes against the gram-positive *S. aureus* on all 7 days; against the gram-negative *S. entiritidis* on day 3 for the composite HAp paste containing 19.4 wt.% gelatin and days 1-2 and 6-7 for the HAp composite containing 26.5 wt.% gelatin; against *S. liquefaciens* on days 2 through 6; and against *P. aeruginosa* on days 1, 2, 3 and 7 for the HAp composite containing 19.4 wt.% gelatin and on all 7 days for the HAp composite containing 26.5 wt.% gelatin (Figs.10-11). The antibacterial effects of pure, antibiotic-free composite pastes were detected, but to a minor extent compared to the self-setting pastes composed of HAp only and no gelatin-silica hybrid reported in our previous study. Clearly, the antimicrobial effects of HAp pastes are, therefore, attributable to an interaction between HAp nanoparticles and the bacterial cells, which becomes minimized following the encapsulation of HAp nanoparticles in gelatin-silica matrix and their effective shielding from a direct contact with the bacteria. With the biological interactions depending on the properties and the physical makeup of both entities in interaction, it does not come as a surprise that the antibacterial effect of the pure composite pastes, containing no antibiotics, were highly bacterium-dependent. Thus, whereas the bacteriostatic effect of the pastes was pronounced against *S. liquefaciens* and *E. coli*, it was present only at the earliest time points when tested against *S. aureus*, *S. enteritidis*, *P. aeruginosa*. With *S. aureus* being a gram-positive bacterium and *S. enteritidis* and *P. aeruginosa* being gram-positive bacteria, it is clear that the gram positive/negative dichotomy cannot be used in the context of explaining the antibacterial activity of the pastes. Interestingly, whereas the bacterial count of *S. enteritidis* and *P. aeruginosa* was reduced significantly for HAp pastes with 19.4 wt.% gelatin

after days 1 – 2 and day 1, respectively (Fig.10), no significant reduction in the bacterial concentration was observed when the same assay was run with HAp pastes containing 26.5 wt.% gelatin (Fig.11). This is another direct evidence that the antibacterial effects of the composite pastes are due to interaction between HAp nanoparticles and the bacteria, which becomes mitigated when the nanoparticles become coated by gelatin-silica.
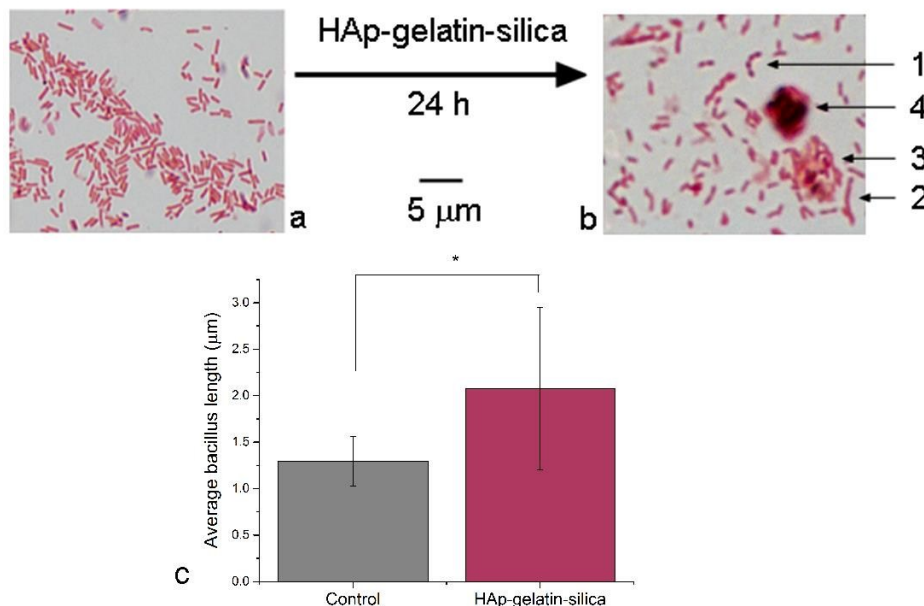

Fig.12. Optical images (a, b) and median lengths (c) of gram-stained *S. liquefaciens* bacilli having undergone no treatment (a) and having been treated with HAp-gelatin-silica pastes. The destruction of bacteria proceeds in the following steps: (1) filamentation through the formation of dimers and multimers; (2) increase in the filament aspect ratio; (3) extensive aggregation; and (4) formation of necrotic spheroids. Data in (c) are shown as averages with error bars representing standard deviation. The asterisk denotes an extremely statistically significant difference (P < 0.0001).

A comparison between the activity of pure vancomycin and vancomycin-loaded pastes led to the observation of the ability of the pastes to augment the activity of vancomycin against specific types of bacteria, such as *P. aeruginosa* (days 1 and 2 for both HAp composite with 19.4 wt.% gelatin and HAp composite with 26.5 wt.% gelatin), *E. coli* (days 2 to 3 for the HAp composite with 19.4 wt.% gelatin), and *S. liquefaciens* (days 1 through 6 for the HAp composite with 19.4 wt.% gelatin). The most intense antibacterial activity augmentation effect was seen against *S. liquefaciens*, evident at all but the last, 7th day of the incubation time (Fig.10c). The treatment with pure vancomycin had no effect on the bacterial count in the broths, but the treatment with the pure composite pastes as well as with the vancomycin-loaded ones was able to keep the bacterial concentration reduced for 3 and 6 days, respectively (Fig.10c). Following the interaction with the composite pastes, *S. liquefaciens* bacilli undergo filamentation (Fig.12a-b) and the average length of the viable bacteria, as shown in Fig.12c, changes from 1.3 to 2.1. In contrast to the rounding of bacilli, which is the result of inhibited lateral wall peptidoglycan synthesis and the activation of the septal wall peptidoglycan synthesis, their elongation is caused by the opposite effect. The observed morphological changes thus indicate an effect on the cell wall as a possible mechanism of action of the composite pastes. This is additionally supported by the fact that cell wall inhibitors are typified by the formation of multimers in a stage preceding the filamentation[52]. Bacterial elongation as the result of disrupted proteoglycan synthesis is a natural defense mechanism against stress-inducing physicochemical agents, given that lengthened cells are more difficult to ingest

and phagocytose by neutrophils[53]. As shown in Fig.12, the beading of the bacilli is succeeded by the formation of continuous filaments and then by aggregation, lysis and formation of necrotic spheroplasts, the transition to which increases with the duration of the treatment[54]. The inhibition of penicillin-binding protein 3, which crosslinks proteoglycan exclusively at the septal, but not the lateral wall, the inhibition of DNA synthesis through the SOS response and the inhibition of protein and/or RNA syntheses have all been invoked as possible downstream causes of bacterial filamentation[55].

Previous studies have shown that HAp can destroy the cell wall of bacteria and induce K^+ leakage, resulting in cell death[56]. This could be the mechanism by which the combination of HAp as a carrier and vancomycin as the drug acts synergistically, endowing the antibiotic with a greater antibacterial efficacy than that typifying it alone. The increased apoptotic effects of chemotherapeutics following their delivery using CP nanoparticles were reported before[57,58,59,60] and were attributed to other possible causes, including the sustained drug release enabled by the CP carrier and the excessive calcium ion release[61,62] capable of triggering the caspase-dependent apoptotic pathway[63,64] by permeabilizing the mitochondrion[65]. However, if the release of ions, most critically Ca^{2+}, is accepted as the mechanism for the augmentation of the toxic effect HAp particles have on microorganisms, it would be difficult to explain numerous cases where modifications of HAp particle properties affected the cell response even when their degradation rates did not significantly change. One example comes from a study in which the particle size of HAp affected the cell viability in such a way that 45 nm particles were more toxic than either 26 nm or 78 nm ones[66]. This is why we hypothesize that the penetration of the cell wall and the intracellular delivery of the antibiotic is the key to explaining the augmented antibacterial activity promoted by HAp as a carrier. This agrees with our previous finding of enhanced antimicrobial efficacy of clindamycin against intracellular colonies of *S. aureus* following the delivery of the drug using HAp nanoparticles as the carrier[67]. In this study, too, we see that the delivery of vancomycin using HAp nanoparticles can significantly augment the efficacy of the antibiotic *per se*. This is especially interesting when it is noted that vancomycin is an antibiotic with little to no efficacy against gram-negative bacteria in the first place[68].

Finally, experiments assessing the interaction of the pastes with healthy cells indicated that the addition of the vancomycin-carrying composite pastes to cultured hMSCs had no negative effects on their viability. As seen from Fig.13, no reduction in viability was observed in cultures treated with the composite HAp pastes containing either 19.4 or 26.5 wt.% gelatin. Additionally, the composite pastes were more abundantly uptaken by the hMSCs than pure HAp. As shown in Fig.14f, the uptake of the composite paste was three times higher than that of pure HAp. This effect in theory favors the use of the composite paste as a gene carrier over pure HAp and may be due to a greater degree of cohesiveness in the composite paste, which prevents the dissipation of particles optimally sized for the uptake (~ 200 nm, Fig.1b) into overly fine, sub-20-nm sized HAp units (Fig.2a). Another possibility is that gelatin engages in interaction with Endo180, a member of the mannose receptor family, which activates the endocytic uptake pathway in fibroblastic cells and facilitates the cellular internalization of the material[69]. Endo180 is a urokinase plasminogen activator receptor-associated protein that is expressed in all bone-forming tissues, mature and immature[70]. It binds through its fibronectin type II domain to both native and denatured collagens and activates their uptake via a clathrin-dependent pathway[71]. A more passive effect contributing to the grater uptake of gelatin-containing particles may be also due to their larger adhesiveness in contact with the cell surface compared to pure HAp. Furthermore, endocytic uptake pathways could be triggered indirectly, thanks to the nonspecific binding of gelatin to integrins $\alpha_2\beta_1$ and

$\alpha_3\beta_1$, discoidin domain receptors, glycoprotein VI, collagen scavenger or other cell membrane receptors[72,73]. Meanwhile, no morphological abnormalities were detected in hMSCs following their treatment with either pure HAp (Fig.14b-c) or the composite paste (Fig.14d-e) when compared to the untreated control (Fig.14a). This selectivity exhibited by the pastes, toxic for the bacteria and harmless for the primary stem cells, is a promising property when it comes to their consideration for application as bone grafts in the treatment of osteomyelitis.
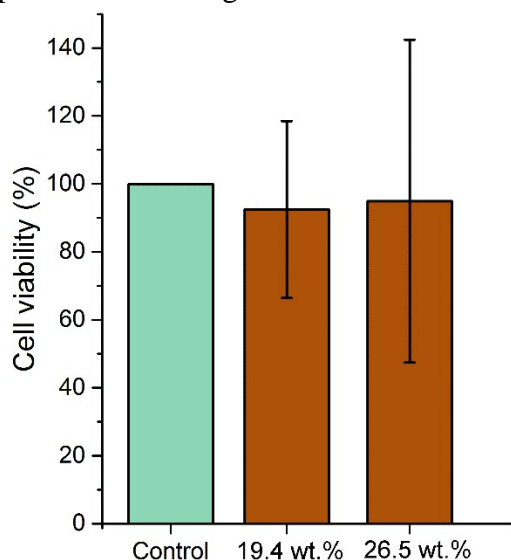

Fig.13. hMSC viability following the treatment with the vancomycin-loaded composite HAp-gelatin-silica pastes containing different amounts of gelatin: 19.4 and 26.5 wt.%. Bars represent averages, while error bars are standard deviations. No statistically significant difference ($p < 0.05$) is detected between any of the sample groups.
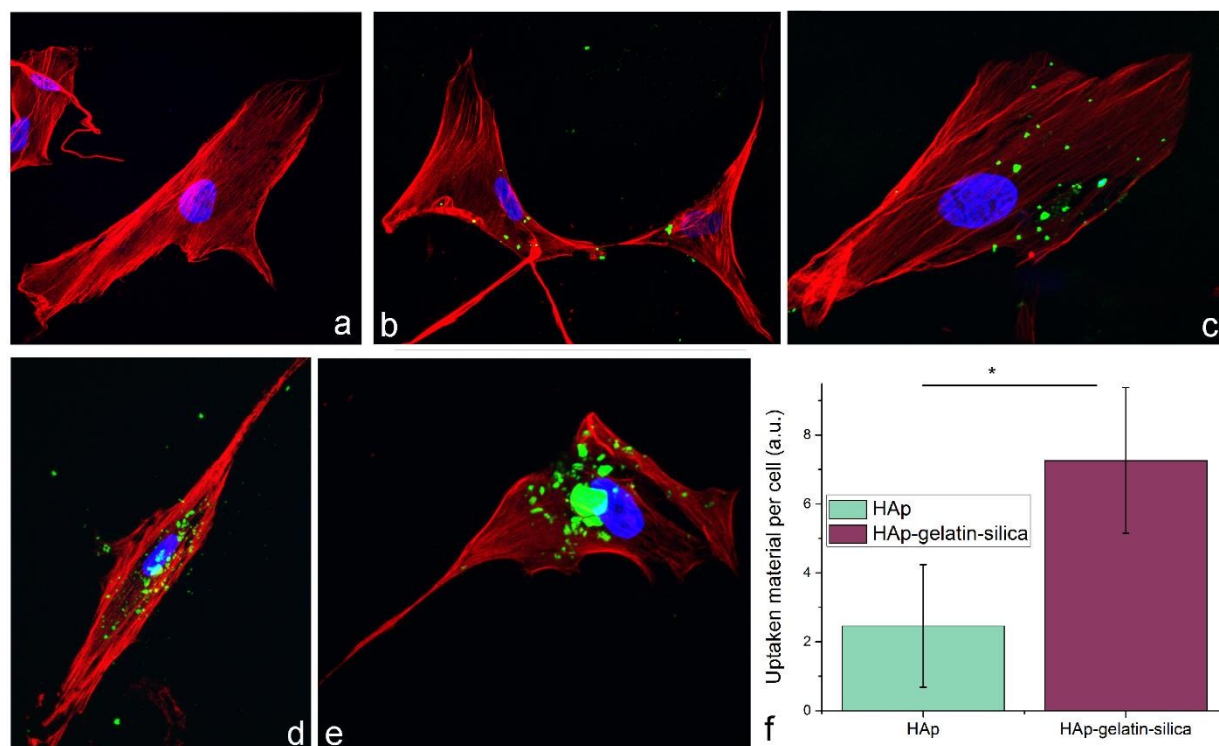
Fig.14. Confocal fluorescent optical images showing hMSCs subjected to no treatment (a) and challenged with either a pure HAp paste (b-c) or a composite HAp-gelatin-silica paste. Cells were stained for nucleus (blue) and f-actin cytoskeletal microfilaments (red), while the nanomaterial was stained in green. Data in (f) represent a difference in the amount of uptaken material per cell and are shown as averages with error bars representing standard deviation. The asterisk denotes an extremely statistically significant difference ($P < 0.001$).

4. Conclusion

In this study we report on a bioresorbable composite material that is compact, yet flowing upon injection; that promotes antibacterial activity while being harmless to healthy cells; that forms pores large enough to accommodate cells inside its structure following immersion in body fluids; and that sets under physiological conditions in a tunable manner and in clinically relevant time windows, ranging from 1 to 3 minutes at its fastest, while delaying the setting under ambient conditions. In spite of these promising properties, the composite pastes display deficiencies that must be solved, including, most critically, the weak mechanical properties and phase segregation during flow. The former, mechanical stability issue is tied to the unanswered problem of integration of HAp crystals into collagen fibers on the nano scale, without which no replication of the mechanical properties of bone is possible. Therefore, introduction of a proper bridging agent, acting as a link between CP crystals and gelatin and ensuring a uniform bonding conformation, may be a next logical step in the design of these composites. The stability issue during flow, in turn, has origins in the inherently weak colloidal stability of CP nanoparticles, caused in part by their inherently low zeta potentials and in part by the highly hydrated and diffusive surface that fosters Ostwald ripening and other forms of aggregational growth. It calls for the use of appropriate surfactants, though such that will not interfere with the particle-particle contact on which the successful setting reaction depends. Integration of stable porogens, whose dissolution would create interconnected pores in the material while sustaining the macroporous structure against its tendency to collapse and crumble, is another tremendous challenge that needs to be solved.

The findings of this study fall along the line of effort to use nanoparticles to augment the activity of pharmacotherapies that may have lost or never had any efficacy against certain pathologies. Specifically, we have shown that composite CP pastes can increase the activity of antibiotics compared to the antibiotic therapy alone. This includes the types of bacteria resistant to the delivered antibiotic, vancomycin, because of their outer membrane impermeability to it. Observation of this effect, which may be due to the bacterial cell wall disruption enabled by CP nanoparticles, reinforces our belief that CP nanoparticles present a viable carrier of antibiotics for a range of infections, extending beyond the realm of bone and other hard tissues. These findings are expected to be a rivulet transformable into a grand stream of effort to augment or completely eliminate the need for pharmacologically active molecules by utilizing the knowledge of materials chemistry to rationally design nanoparticulate materials with well-defined biomedical properties.
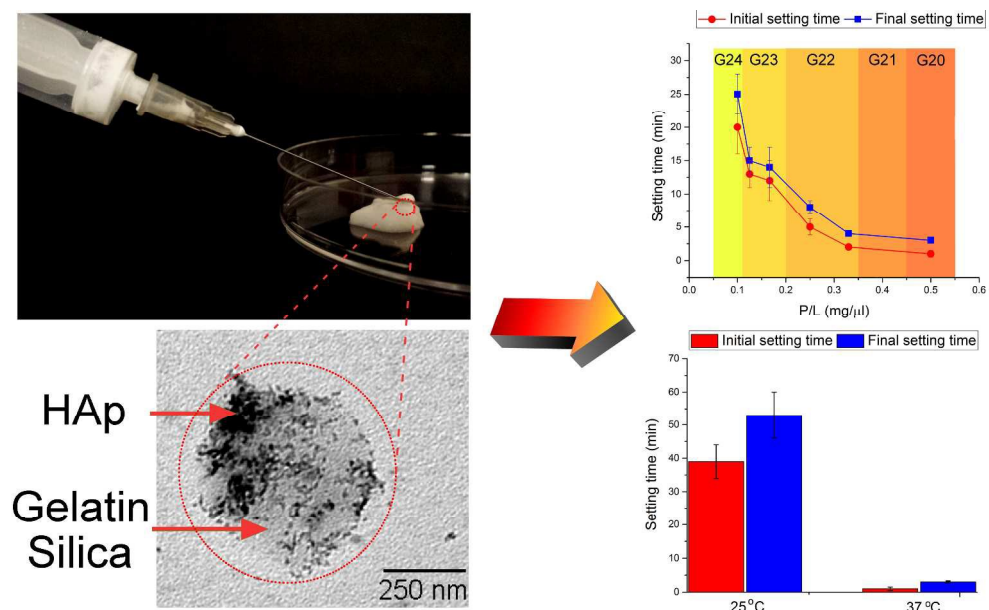
5. Acknowledgements

6. References

[1] K. R. Fingar, C. Stocks, A. J. Weiss, C. A. Steiner, Most Frequent Operating Room Procedures Performed in U. S. Hospitals, 2003 – 2012: Statistical Brief #186", Healthcare Cost and Utilization Project (HCUP) Statistical Briefs [Internet]. Rockville (MD): Agency for Healthcare Research and Quality (US); 2014.

[2] V. Uskoković – "When 1 + 1 > 2: Nanostructured Composite Materials for Hard Tissue Engineering Applications", Materials Science and Engineering C: Materials for Biological Applications 57, 434 – 451 (2015).

[3] I. Dumic-Cule, M. Pecina, M. Jelic, M. Jankolija, I. Popek, L. Grgurevic, S. Vukicevic – "Biological aspects of segmental bone defects management", Int. Orthop. 39, 1005 – 11 (2015).

[4] A. Ahgazadeh, G. Ruther Persson, S. Renvert – "A single-centre randomized controlled clinical trial on the adjunct treatment of intra-bony defects with autogenous bone or a xenograft: results after 12 months", J. Clin. Periodontol. 39, 666 – 673 (2012).

[5] F. D. Beaman, L. W. Bancroft, J. J. Peterson, M. J. Kransdorf – "Bone graft materials and synthetic substitutes", Radiologic Clinics of North America 44, 451 – 461 (2006).

[6] C. R. Lareau, M. E. Deren, A. Fantry, R. M. Donahue, C. W. DiGiovanni – "Does autogenous bone graft work? A logistic regression analysis of data from 159 papers in the foot and ankle literature", Foot Ankle Surg. 21, 150 – 9 (2015).

[7] J. Dashe, R. L. Parisien, A. Cusano, E. J. Curry, A. Bedi, X. Li – "Allograft tissue irradiation and failure rate after anterior cruciate ligament reconstruction: A systematic review", World J. Orthop. 7, 392 – 400 (2016).

[8] V. Uskoković, D. P. Uskoković – "Nanosized Hydroxyapatite and Other Calcium Phosphates: Chemistry of Formation and Application as Drug and Gene Delivery Agents", Journal of Biomedical Materials Research B: Applied Biomaterials 96B (1) 152 – 191 (2011).

[9] V. Uskoković, T. A. Desai – "Phase Composition Control of Calcium Phosphate Nanoparticles for Tunable Drug Delivery Kinetics and Treatment of Osteomyelitis. I. Preparation and Drug Release", Journal of Biomedical Materials Research Part A 101 (5) 1416 – 1426 (2013).

[10] F. Monchau, Ph. Hivart, B. Genestie, F. Chai, M. Descamps, H. F. Hildebrand – "Calcite as a bone substitute. Comparison with hydroxyapatite and tricalcium phosphate with regard to the osteoblastic activity", Materials Science and Engineering C 33, 490 – 498 (2013).

[11] M. Houmard, Q. Fu, M. Genet, E. Saiz, A. P. Tomsia – "On the structural, mechanical, and biodegradation properties of HA/β-TCP robocast scaffolds", J Biomed Mater Res B: Appl. Biomater 101, 1233 – 1242 (2013).

[12] S. V. Dorozhkin, Self-Setting Calcium Orthophosphate Formulations. J. Funct. Biomater. 2013, 4 (4), 209–311.

[13] Y. Fukase, E. D. Eanes, S. Takagi, L. C. Chow, W. E. Brown, Setting reactions and compressive strengths of calcium phosphate cements. J. Dent. Res. 1990, 69, 1852-1856.

[14] H. Yuan, Y. Li, J. D. de Bruijn, K. de Groot, X. Zhang – "Tissue Response of Calcium Phosphate Cement: A Study in Dogs", Biomaterials 21, 1283 – 1290 (2000).

[15] Y. Miyamoto, K. Ishikawa, M. Takeshi, T. Toh, Y. Yoshida, M. Nagayama, M. Kon, K. Asaoka, Tissue response to fast-setting calcium phosphate cement in bone. J. Biomed. Mater. Res. 1997, 37, 457-464.

[16] J. An, H. Liao, N. W. Kucko, R. P. Herber, J. G. Wolke, J. J. van den Beucken, J. A. Jansen, S. C. Leeuwenburgh, Long-term evaluation of the degradation behavior of three apatite-forming calcium phosphate cements, J Biomed Mater Res A. 2016 May;104(5):1072-81.

[17] G. Iviglia, C. Cassinelli, E. Torre, F. Baino, M. Morra, C. Vitale-Brovarone – "Novel bioceramic-reinforced hydrogel for alveolar bone regeneration", Acta Biomaterialia, in press (2016).

[18] V. Uskoković – "Nanostructured Platforms for the Sustained and Local Delivery of Antibiotics in the Treatment of Osteomyelitis", Critical Reviews in Therapeutic Drug Carrier Systems 32 (1) 1 – 59 (2015).

[19] S. Ghosh, V. M. Wu, S. Pernal, V. Uskoković – "Self-Setting Calcium Phosphate Cements with Tunable Antibiotic Release Rates for Advanced Bone Graft Applications", ACS Applied Materials and Interfaces 8 (12) 7691 - 7708 (2016).

[20] A. Yenson, H. O. de Fries, Z. E. Deeb, Actinomycotic osteomyelitis of the facial bones and mandible. Otolaryngol Head Neck Surg 1983;91(2):173-6.

[21] J. Hatzenbuehler, T. J. Pulling, Diagnosis and management of osteomyelitis. Am Fam Physician 2011;84(9)1027–33.

[22] J. D. Pasteris, B. Wopenka, E. Valsami-Jones – "Bone and Tooth Mineralization: Why Apatite?, Elements 4, 97 – 104 (2008).

[23] S. Panseri, M. Montasi, S. M. Dozio, E. Savini, A. Tampieri, M. Sandri – "Biomimetic scaffold with aligned microporosity designed for dentin regeneration", Front Bioeng Biotechnol 4, 48 (2016).

[24] V. Uskoković, N. Ignjatović, N. Petranović – "Synthesis and Characterization of Hydroxyapatite-Collagen Biocomposite Materials", Materials Science Forum 413, 269 – 274 (2003).

[25] V. Guarino, M. Alvarez-Perez, V. Cirillo, L. Ambrosio – "hMSC interaction with PCL and PCL/gelatin platforms: A comparative study on films and electrospun membranes", Journal of Bioactive and Compatible Polymers 26, 144-160 (2011).

26 A. N. Shirazi, A. Fathi, F. G. Suarez, Y. Wang, P. K. Maitz, F. Dehghani – "A Novel Strategy for Softening Gelatin-Bioactive-Glass Hybrids", ACS Applied Materials and Interfaces 8, 1676 – 86 (2016).

27 O. Mahony, S. Yue, C. Turdean-Ionescu, J. V. Hanna, M. E. Smith, P. D. Lee, J. R. Jones – "Silica-gelatin hybrids for tissue regeneration: inter-relationships between the process variables", J Sol Gel Sci Technol 69, 288 – 198 (2014).

28 R. Gillani, B. Ercan, A. Qiao, T. J. Webster – "Nanofunctionalized zirconia and barium sulfate particles as bone cement additives", Int. J. Nanomed. 5, 1 – 11 (2010).

29 K. Goto, J. Tamura, S. Shinzato, S. Fujibayashi, M. Hashimoto, M. Kawashita, T. Kokubo, T. Nakamura – "Bioactive bone cements containing nano-sized titania particles for use as bone substitutes", Biomaterials 26, 6496 – 6505 (2005).

30 V. Uskoković – "Dynamic Light Scattering and Microelectrophoresis: Main Prospects and Limitations", Journal of Dispersion Science and Technology 33 (12) 1762 – 1786 (2012).

31 E.B. Montufar, T. Traykova, E. Schacht, L. Ambrosio, M. Santin, J.A. Planell, M.-P. Ginebra – "Self-hardening Calcium Deficient Hydroxyapatite/Gelatine Foams for Bone Regeneration", J. Mater. Sci.: Mater. Med., 21 (2010), pp. 863–869.

32 D. W. Dempster, E. Shane, Bone Quantification and Dynamics of Turnover, In: Principles and Practice of Endocrinology and Metabolism, Third Edition, edited by K. L. Becker, Lippincott Williams & Wilkins, Philadelphia, PA, 2001, pp. 541 – 547.

33 V. Uskoković, S. Ghosh – "Carriers for the Tunable Release of Therapeutics: Etymological Classification and Examples", Expert Opinion on Drug Delivery 13 (12) 1729 – 1741 (2016).

34 A. K. Philip, B. Philip – "Chronopharmaceuticals: hype or future of pharmaceutics", Curr Pharm Des 17, 1512 – 6 (2011).

35 H. Unuma, Y. Matsushima – "Preparation of Calcium Phosphate Cement with an Improved Setting Behavior", Journal of Asian Ceramic Societies 1, 26 – 29 (2013).

36 S. Hesaraki, M. Alizadeh, S. Borhan, M. Pourbaghi-Masouleh – "Polymerizable nanoparticulate silica-reinforced calcium phosphate bone cement", J. Biomed. Mater. Res. B 100, 1627 – 1635 (2012).

37 Y. J. No, S. I. Roohani-Eshafani, H. Zreiqat – "Nanomaterials: The Next Step in Injectable Bone Cements", Nanomedicine (London) 9, 1745 – 1764 (2014).

38 W. R. Stoll, W. F. Neuman – "The Uptake of Sodium and Potassium Ions by Hydrated Hydroxyapatite", Journal of the American Chemical Society 78, 1585 – 1588 (1956).

39 D. G. A. Nelson – "The Influence of Carbonate on the Atomic Structure and Reactivity of Hydroxyapatite", J. Dent. Res. 60C, 1621 (1981).

40 D. G. A. Nelson, J. D. B. Featherstone, J. F. Duncan, T. W. Cutress – "Paracrystalline disorder of biological and synthetic carbonate-substituted apatites", J. Dent. Res 61, 1274 (1982).

41 K Maruta, K. Ichimura, H. Matsui, T. Yamagami, A. Sano, H. Tsuji – "Calcificationn Inhibitors in Human Ligamentum Flavum", J Orthop Res 11, 92 – 103 (1993).

42 W. Kunz – "Specific Ion Effects in Colloidal and Biological Systems", Current Opinion in Colloid & Interface Science 15 (2010) 34–39.

43 S. del Valle, N. Miňo, F. Muňoz, A. Gonzalez, J. A. Planell, M. P. Ginebra, In vivo evaluation of an injectable macroporous calcium phosphate cement. J. Mater. Sci. Mater. Med. 2007, 18, 353-361

44 B. Feng, M. Guolin, Y. Yuan, L. Changshen, W. Zhen, L. Jian, Role of macropore size in the mechanical properties and in vitro degradation of porous calcium phosphate cements. Mater. Lett. 2010, 64, 2028-2031

[45] V. B. Fedoseev, M. V. Maksimov – "Solution-Crystal-Solution Oscillatory Phase Transitions in the KCl-NaCl-H_2O System", JETP Letters 101, 390 – 3 (2015).

[46] I. G. Kovzun, N. V. Pertsov – "Colloid Chemical Processes of Contact Self-Organization in Alkaline Silicate Composites and Their Relation to Formation of Nanosized Surface Structures", In: Nanoscience: Colloidal and Interfacial Aspects, edited by Victor M. Starov, Surface Science Series 147, CRC Press, Boca Raton, FL (2010), pp. 527.

[47] P. Ball, Forging Patterns and Making Waves from Biology to Geology: A Commentary on Turing (1952) 'The Chemical Basis of Morphogenesis'. Phil. Trans. Royal Soc. B 2015, 370, 1 – 10.

[48] K. W. Kolasinski – "Surface Science: Foundations of Catalysis and Nanoscience", Third edition, Wiley, Chichester, UK (2012), pp. 293.

[49] C. L. Charlton, J. A. Hindler, J. Turnidge, R. M. Humphries – "Precision of Vancomycin and Daptomycin MICs for Methicillin-Resistant Staphylococcus aureus and Effect of Subculture and Storage", J. Clin. Microbiol. 52, 3898 – 3905 (2014).

[50] R. S. Kalhapure, N. Suleman, C. Mocktar, N. Seedat, T. Govender, Nanoengineered drug delivery systems for enhancing antibiotic therapy", J Pharm Sci 104(3):872-905 (2015).

[51] A. L. Armstead, B. Li – "Nanomedicine as an emerging approach against intracellular pathogens", Int J Nanomedicine 6, 3281 – 93 (2011).

[52] P. Nonejuie, M. Burkart, K. Pogliano, J. Pogliano – "Bacterial cytological profiling rapidly identifies the cellular pathways targeted by antibacterial molecules", Proc Natl Acad Sci USA 40, 16169 – 16174 (2013).

[53] S. S. Justice, C. Hung, J. A. Theriot, D. A. Fletcher, G. G. Anderson, M. J. Footer, S. J. Hultgren, Differentiation and developmental pathways of uropathogenic Escherichia coli in urinary tract pathogenesis, Proc Natl Acad Sci USA 101:1333–1338 (2004).

[54] T. S. J. Elliott, D. Greenwood – "The response of Pseudomonas aeruginosa to azlocillin, ticarcillin and cefsulodin", J Med Microbiol 16:351–362 (1983).

[55] T. P. T. Cushnie, N. H. O'Driscoll, A. J. Lamb – "Morphological and ultrastructural changes in bacterial cells as an indicator of antibacterial mechanism of action", Cell. Mol. Life Sci. 73, 471 – 4492 (2016).

[56] P. N. Lim, L. Chang, B. Y. Tay, V. Guneta, C. Choong, B. Ho, E. S. Thian Proposed Mechanism of Antibacterial Action of Chemically Modified Apatite for Reduced Bone Infection, ACS Appl. Mater. Interfaces, 2014, 6 (19), pp 17082–17092.

[57] X. Cheng, L. Kuhn – "Chemotherapy drug delivery from calcium phosphate nanoparticles", Int J Nanomedicine 2 (4), 667 – 74 (2007).

[58] M. Kester, Y. Heakal, T. Fox, A. Sharma, G. P. Robertson, T. T. Morgan, E. I. Altinoglu, A. Tabakovic, M. R. Parette, S. M. Rouse, V. Ruiz-Velasco, J. H. Adair – "Calcium phosphate nanocomposite particles for in vitro imaging and encapsulated chemotherapeutic drug delivery to cancer cells", Nano Lett 8 (12), 4116 – 21 (2008)

[59] S. H. Chu, D. F. Feng, Y. B. Ma, Z. Q. Li – "Hydroxyapatite nanoparticles inhibit the growth of human glioma cells in vitro and in vivo", Int J Nanomedicine 7, 3659 – 66 (2012)

[60] Y. Luo, Y. Ling, W. Guo, J. Pang, W. Liu, Y. Fang, X. Wen, K. Wei, X. Gao – "Docetaxel loaded oleic acid-coated hydroxyapatite nanoparticles enhance the docetaxel-induced apoptosis through activation of caspase-2 in androgen independent prostate cancer cells", J Control Release 43 (2), 278 – 88 (2010)

[61] R. Meena, K. Kesari, M. Rani, R. Paulraj – "Effects of hydroxyapatite nanoparticles on proliferation and apoptosis of human breast cancer cells (MCF-7)", Journal of Nanoparticle Research 14 (2), 1 (2012)

[62] A. E. Ewence, M. Bootman, H. L. Roderick, J. N. Skepper, G. McCarthy, M. Epple, M. Neumann, C. M. Shanahan, D. Proudfoot – "Calcium phosphate crystals induce cell death in human vascular smooth muscle cells: a potential mechanism in atherosclerotic plaque destabilization", Circ Res 103 (5), e28 – 34 (2008)

[63] F. Ichas, J. P. Mazat – "From calcium signaling to cell death: two conformations for the mitochondrial permeability transition pore. Switching from low- to high-conductance state", Biochim Biophys Acta 1366 (1-2), 33 – 50 (1998).

[64] M. Pourbaghi-Masouleh, V. Hosseini – "Amorphous calcium phosphate nanoparticles could function as a novel cancer therapeutic agent by employing a suitable targeted drug delivery platform", Nanoscale research letters 8 (1), 449 (2013).

[65] Y. Sun, Y. Chen, X. Ma, Y. Yuan, C. Liu, J. Kohn, J. Qian – "Mitochondria-Targeted Hydroxyapatite Nanoparticles for Selective Growth Inhibition of Lung Cancer in Vitro and in Vivo", ACS Applied Materials and Interfaces 8, 25680 – 25690 (2016).

[66] Y. Yuan, C. Liu, J. Qian, J. Wang and Y. Zhang – "Size-mediated cytotoxicity and apoptosis of hydroxyapatite nanoparticles in human hepatoma HepG2 cells", Biomaterials 31 (4), 730 (2010).

[67] V. Uskoković, T. A. Desai – "Simultaneous Bactericidal and Osteogenic Effect of Nanoparticulate Calcium Phosphate Powders Loaded with Clindamycin on Osteoblasts Infected with Staphylococcus Aureus", Materials Science and Engineering C: Materials for Biological Applications 37, 210 – 222 (2014).

[68] M. H. McCormick, J. M. McGuire – "Vancomycin and method for its preparation", US Patent 3,067,099 (1962).

[69] L. East, C. M. Isacke, The mannose receptor family, Biochim Biophys Acta 1572(2-3):364-86 (2002).

[70] L. H. Engelholm, B. S. Nielsen, S. Netzel-Arnett, H. Solberg, X. D. Chen, J. M. Lopez Garcia, C. Lopez-Otin, M. F. Young, H. Birkedal-Hansen, K. Danø, L. R. Lund, N. Behrendt, T. H. Bugge, The urokinase plasminogen activator receptor-associated protein/endo180 is coexpressed with its interaction partners urokinase plasminogen activator receptor and matrix metalloprotease-13 during osteogenesis", Lab Invest. 2001;81(10):1403-14.

[71] D. Wienke, J. R. MacFadyen, C. M. Isacke – "Identification and Characterization of the Endocytic Transmembrane Glycoprotein Endo180 as a Novel Collagen Receptor", Mol Biol Cell 14, 3592 – 3604 (2003).

[72] W. F. Vogel, A. Aszódi, F. Alves, T. Pawson, Discoidin domain receptor 1 tyrosine kinase has an essential role in mammary gland development", Mol Cell Biol. 2001 Apr; 21(8):2906-17.

[73] N. Ikenaga, Ohuchida K, Mizumoto K, Akagawa S, Fujiwara K, Eguchi D, Kozono S, Ohtsuka T, Takahata S, Tanaka M. – "Pancreatic cancer cells enhance the ability of collagen internalization during epithelial-mesenchymal transition", PLoS One 7(7):e40434 (2012).

1066x649mm (72 x 72 DPI)